DESIGN AND ANALYSIS OF A MULTI-CELL SUBSCALE TANK FOR LIQUID HYDROGEN STORAGE

Ilias G. Tapeinos[1], Sotiris Koussios[1] and Roger M. Groves[2]

[1]Structural Integrity & Composites Group, Faculty of Aerospace Engineering,
Delft University of Technology, Kluyverweg 1, 2629HS Delft, Netherlands
[2]Aerospace Non-Destructive Testing Laboratory, Faculty of Aerospace Engineering,
Delft University of Technology, Kluyverweg 1, 2629HS Delft, Netherlands

Email: I.Tapeinos@tudelft.nl, web page: http://www.tudelft.nl/

Keywords: Conformable tanks, Thermal stresses, Finite element method

ABSTRACT

This paper outlines the structural performance of a conformable pressurizable tank consisting of intersecting spherical shells (multi-cell tank). Multi-cell tanks outrival conventional multiple cylindrical tanks in volumetric efficiency when required to fit in a rectangular envelope in the automotive industry. When pressurized, the multi-cell (or multi-bubble) tank experiences high stress concentrations at the vicinity of the junctions, and thus the concept of effectively reinforcing those regions without adding significant excess weight becomes crucial. Furthermore when applied for cryogenic medium storage the heat transfer between different bodies and generation of respective thermal stresses in such vessels makes the solution more complicated. In this paper the effect of the i) fiber-reinforced materials at the membrane and ii) unidimensional carbon tows at the intersections on the structural integrity of the tank is analyzed for different loading scenarios.

1 INTRODUCTION

In the aerospace hydrogen containment field, tanks are required to have of high internal volume, in a pre-defined allowable space. The EU CHATT (Cryogenic Hypersonic Advanced Tank Technologies) project deals with investigating the use of carbon-fibre reinforced plastics (CFRP) for type IV liquid hydrogen (LH_2) tanks in the two-stage hypersonic reusable launch system (RLV) Space-Liner [1]. Throughout operation the tank is subjected to various combined loading cases that involve inner pressure and temperature changes as well as gravitational accelerations induced by the RLV.

Multi-cell pressure vessels have shown potential of higher volumetric efficiency compared to conventional cylindrical tanks, since the main rationale is to maximize their internal volume [2]. They consist of rows of spherical cells joined together at appropriate intersections. Spherical membrane cells enable the structure to be loaded in uniform equal biaxial tension, which enables structural efficiency maximization [3]. The use of intersecting spherical pressure tanks has been reported in several published works [4]-[5]. However the application of fiber-reinforced materials for multi-cell vessels employed for storing liquid mediums at cryogenic temperatures has not yet been realized.

In order to prevent gas diffusion through the wall, composite overwrapped pressure vessels typically have a liner. However, differences in the values of the coefficient of thermal expansion (CTE), between the liner and the wall can lead to thermal stresses under a temperature gradient. Therefore besides permeability resistance, the two driving properties for liner material selection are i) the CTE compatibility with the composite tank wall and ii) the specific modulus since the liner must not enter the plastic zone nor add significant excess weight.

In the present work, a trade-off design study of plastic-lined multi-cell tank concepts has been performed in terms of evaluating their structural performance, under a given loading scenario, both analytically and with the use of Finite Element Analysis (FEA). The polymer material utilized at the liner, was polyoxymethylene (POM). The effect of the intersection reinforcement-under consideration

on the tank behavior was evaluated. Furthermore, a coupled temperature-displacement FE analysis was employed to investigate heat transfer phenomena between the liner and the tank wall, as well as to evaluate respective thermal stresses. Finally, a failure three-dimensional envelope for thermo-mechanical loading was established for the proposed tank design indicating the safe zone where the tank can operate freely.

2 TANK OPERATION REQUIREMENTS

To ensure safety and acceptance, pressurized fuel tanks are always subject to strict design and verification requirements. Throughout operation in the Space-Liner the LH_2 tank is to be subjected to various combined loading cases such as inner pressure and temperature change –due to the stored medium at cryogenic temperatures- as well as gravitational accelerations induced by the RLV [6].

Figure 1 depicts the different loading scenarios induced at the tank throughout the RLV flight, which were considered as reference in this study (simplified case). These load cases are associated with i) nominal cryogenic operation at maximum expected temperature or ii) nominal empty operation after main-engine-cut-off (MECO) and iii) off-nominal operation after early MECO with remaining LH_2 inside. The service pressure of 380 [kPa] along with a safety factor of 1.5 resembles the most significant tank design constraint. An integral part of the design is to reinforce the tank, in order to be able to withstand service loads. The application of CFRP at the tank wall will provide support to the structure, due to its high specific strength and stiffness. Additional loading comes from quasi-static inertia loads (n_z or n_x = 2.5 [g] for the worst case scenario), and thus generally needs to be considered throughout a design procedure (Figure 1).

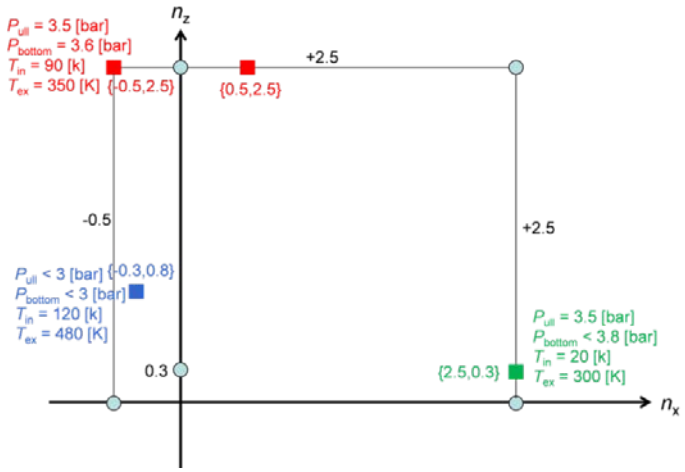

Figure 1: Simplified flight load cases of the Space Liner LH_2 tank.

Figure 2 shows the expected benefits in terms of volumetric efficiency of the conformable tank concept compared to multiple cylinders in a rectangular envelope in the automotive industry [7]. The cross sections of the tanks are depicted, and for various aspect ratio (envelope length/width) values the conformal vessel concept surpasses the respective cylindrical one in terms of volumetric efficiency. Throughout this study a sub-scale of the actual tank (under consideration) was designed and analyzed as reference.

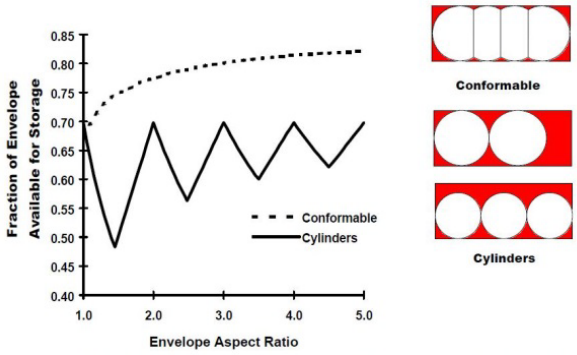

Figure 2: Comparison of the volumetric efficiency between i) cylindrical and ii) conformable tanks in a rectangular envelope [7].

Furthermore, the sub-scale designs must be consistent with the manufacturing processes of the liner and tank wall. More specifically, the external contour of the designed subscale conformal tank must be feasible to manufacture with a rotational moulding process, without inducing any imperfections at narrow sections, such as membrane junctions.

3 SUB-SCALE TANK STRUCTURAL CONFIGURATIONS

This section deals with isolating the different loading scenarios of interest and analyzing their effect on various tank locations of proposed design.

3.1. Spherical Membranes

3.1.1 Mechanical Loading

Figure 3a depicts a conceptual design of the respective structure, which is a quadri-spherical tank, with all centroids in the same plane. As it can be seen in Figure 1, the inner normal pressure induced by the stored liquid medium on the tank wall- can be considered as uniform. The pressure load induced at the vicinity of any intersection is partially carried by the membrane and partially by the reinforcement placed at the intersection, where the stress concentrations obtain their highest values.

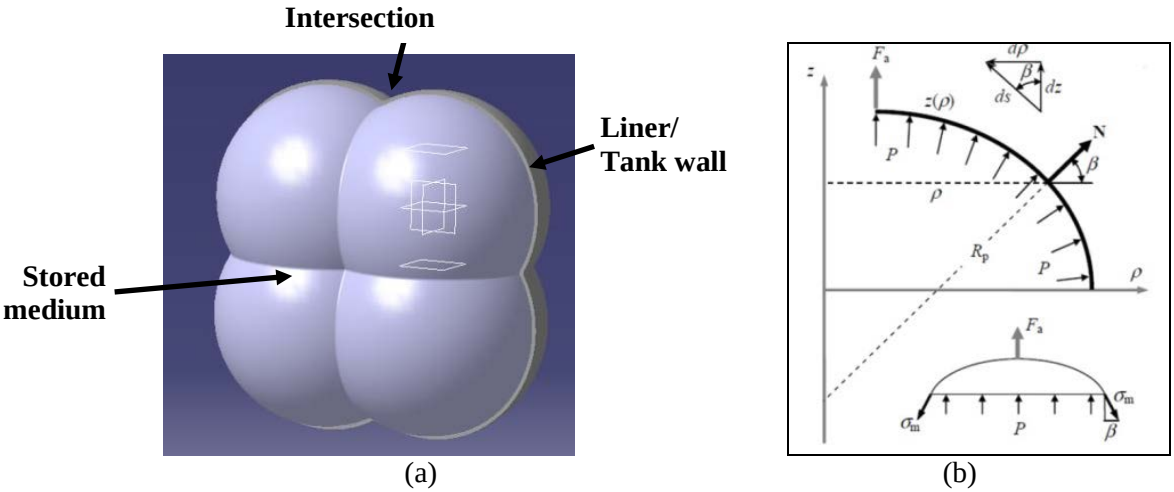

Figure 3: a) Quadri-spherical tank with equal shell radius for all cells and b) stresses equilibrium on a shell of revolution.

The membrane theory for pressure vessels was utilized for the spherical membranes, in order to derive the stress environment of the multi-bubble configuration. It relies on the equilibrium of in-plane stresses on a membrane element by neglecting any bending moments. The average membrane stress

values can be derived by dividing the membrane force with the respective shell thickness. Figure 3b depicts a shell of revolution, which is obtained by rotating a curve (meridian) about an axis of revolution. Therefore an element of the reference surface of the shell is formed by two adjacent meridians and two parallel circles. More specifically, the in-plane equilibrium condition is provided below:

$$\frac{P}{t}=\frac{\sigma_m}{R_m}+\frac{\sigma_p}{R_p} \tag{1}$$

where R_m is the radius of curvature of the meridian, R_p is the radius of curvature in the parallel direction and σ_m, σ_p are the in-plane shell stresses in the meridian and parallel directions respectively. Therefore this case accounts for spherical elements, R_m=R_p. The in-plane shear stress is equal to zero, due to the uniform strain condition. The stiffness matrix of a layer at the tank wall ($\mathbf{C}_o$) would be:

$$\mathbf{C}_o=\begin{pmatrix}\frac{E_x}{1-\nu_{xy}\nu_{xy}} & \frac{\nu_{xy}E_y}{1-\nu_{xy}\nu_{xy}} & 0\\ \frac{\nu_{xy}E_y}{1-\nu_{xy}\nu_{xy}} & \frac{E_y}{1-\nu_{xy}\nu_{xy}} & 0\\ 0 & 0 & G_{xy}\end{pmatrix} \tag{2}$$

where $\nu_{yx}=\frac{\nu_{xy}E_y}{E_x}$ and E_x, E_y and G_{xy} are the ply tensile modulus parallel and transverse to the fibers, and the shear modulus respectively. A quasi-isotropic stacking sequence was chosen ($[0,45,-45,90]_s$). Therefore the resulting stiffness of the laminate will be derived from [8]:

$$\mathbf{C}_{lam}=\frac{1}{\sum_{k=1}^{n}t_{ply}}\cdot\sum_{k=1}^{n}\mathbf{C}(a)\cdot t_{ply} \tag{3}$$

where:

$$\mathbf{C}(a)=\mathbf{M}(a)\cdot\mathbf{C}_o\cdot\mathbf{M}^T(a) \text{ and } \mathbf{M}(a)=\begin{pmatrix}\cos^2 a & \sin^2 a & \sin(2a)\\ \sin^2 a & \cos^2 a & -\sin(2a)\\ -\cos(a)\sin(a) & \cos(a)\sin(a) & \cos(2a)\end{pmatrix} \tag{4}$$

where a represents the different lamina angles, n the number of angles, $\mathbf{M}(a)$ is the transformation matrix and $\mathbf{C}(a)$ is the transformed (reduced) ply stiffness matrix. As a result, the shell stresses vector is given by multiplying the laminate stiffness matrix by the shell strains vector:

$$\begin{Bmatrix}\sigma_m\\ \sigma_p\\ 0\end{Bmatrix}=\mathbf{C}_{lam}\cdot\begin{Bmatrix}\varepsilon_m\\ \varepsilon_p\\ 0\end{Bmatrix} \tag{5}$$

Finally the layer stresses are given by:

$$\begin{Bmatrix}\sigma_1\\ \sigma_2\\ 0\end{Bmatrix}=\mathbf{C}_o\cdot(\mathbf{M}^T(a))^{-1}\cdot\mathbf{S}_{lam}\cdot\begin{Bmatrix}\sigma_m\\ \sigma_p\\ 0\end{Bmatrix} \tag{6}$$

where $S_{lam}=(C_{lam})^{-1}$ is the laminate compliance matrix. Due to axial and shell force equilibrium:

$$\sigma_m = \frac{PR_p}{2t}(F_a + 1)\ ,\ \sigma_p = \sigma_m\left(\frac{2}{F_a + 1} - \frac{R_p}{R_m}\right) \tag{7}$$

where F_a is a dimensionless externally applied axial force on the vessel. Since there is no externally applied force and R_p=R_m for a spherical element, we have $\sigma_m = \sigma_p$.

By utilizing the Tsai-Wu failure criterion (Eq.8) and by using the previous equations in this part of the study, the strength values of the spherical elements can be calculated for the tank wall material and lay-up under consideration:

$$f_1\sigma_1 + f_2\sigma_2 + f_{11}\sigma_1^2 + f_{22}\sigma_2^2 + f_{66}\tau_6^2 + 2f_{12}\sigma_1\sigma_2 = 1 \tag{8}$$

where $f_1 = \frac{1}{X_t} - \frac{1}{X_c}$, $f_{11} = \frac{1}{X_t X_c}$, $f_2 = \frac{1}{Y_t} - \frac{1}{Y_c}$, $f_{22} = \frac{1}{Y_t Y_c}$, $f_{66} = \frac{1}{S^2}$, $f_{12} = -\frac{1}{2}\sqrt{f_{11} f_{22}}$ and respective X_t, X_c, Y_t, Y_c and S ply strength values of the material of interest can be found in Table 1.

ELASTIC					STRENGTH				
E_1 (GPa)	E_2 (GPa)	G_{12} (GPa)	ν_{12}	t_{ply} (mm)	X^t (MPa)	Y^t (MPa)	Y^t (MPa)	Y^c (MPa)	S (MPa)
134.4	12.5	5.31	0.3	0.19	2178.2	1783.5	91.7	340.9	129.1

Table 1: Tank wall material properties (AS4/8552).

3.1.2 Thermal Loading

I. Temperature Distribution

It is of significant importance to calculate the arising temperatures on the spherical cells (liner & tank wall) due to fact that this tank is meant for cryogenic medium storage. More specifically, since the fibre-reinforced composite is draped on the liner and the tank is subjected to different temperatures inside and outside (Figure 2), evaluating the temperature gradient through-the-thickness will enable us to estimate the estimation of heat transfer occurring from one body to another and will aid the calculation of the involved thermal stresses.

When in contact the liner and tank wall tangential behavior at the interface is governed by normal forces and the analysis consists of heat conduction between two bodies. However contact depends on the rate of expansion and contraction of each body which is dominated by the inner pressure, which case will be analyzed in the following sections.

Initially thermal conductivity values of tank wall and liner materials need to be obtained. While the liner material is considered as isotropic, fiber-reinforced materials exhibit anisotropy, with the principal directions of the thermal conductivity being parallel and perpendicular to the fibre orientations. Knowing the thermal conductivity of the fibers and the matrix, the thermal conductivity of a lamina at parallel (along the fibers) and transverse to the fibre directions can be calculated by using the rule of mixtures:

$$k_{II} = (1 - V_f)k_m + V_f k_f\ ,\ k_\perp = \frac{1}{\frac{V_f}{k_f} + \frac{1 - V_f}{k_m}} \tag{9}$$

where k_{II}, $k_\perp$ are the ply-thermal conductivity values in parallel and transverse to fibers directions respectively, k_f, k_m are fibre and epoxy matrix thermal conductivity values and V_f, V_m are the ply fibre and matrix volume fractions respectively (Table 2).

Property	POM	AS4/8552 (Axial)	AS4/8552 (Circ./Thickness)

k	[W K^{-1} m^{-1}]	0.231	3.972	0.3363

Table 2: Thermal Conductivity of various materials.

For the case that the liner and tank wall are tangent to each other, a temperature gradient only through-the thickness (one-dimensional heat transfer) of the spherical cell is considered. For the differential control volume of Figure 4, it is required that $q_r = q_{r+dr}$ for steady-state, one-dimensional conditions with no heat generation, where q_r and q_{r+dr} are heat rates. The appropriate form of Fourier's law is (Figure 4):

$$q_r = -kA\frac{dT}{dr} = -k(4\pi r^2)\frac{dT}{dr} \tag{10}$$

where A is the area normal to heat transfer direction, k is the materials' thermal conductivity and r is the radius at any given point through-the-thickness of the sphere. Since for steady-state conditions q_r is constant and independent of r the equation above can be expressed in its integral form (steady-state conditions); assuming that k is constant:

$$q_r = \frac{4\pi k(T_{s,1} - T_{\infty,2})}{\left(1/r_1\right) - \left(1/r_2\right)} \tag{11}$$

where $A = 4\pi r^2$ is the area normal to the direction of heat transfer.

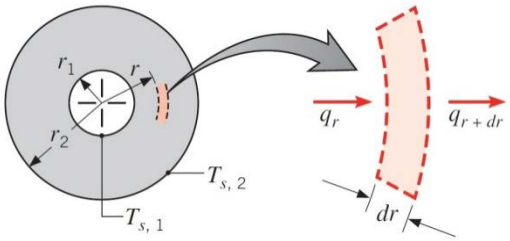

Figure 4: Conduction in a spherical shell.

II. Thermal Stresses

This section deals with analyzing the tank wall thermal stresses. As mentioned above, a linear temperature distribution is expected, associated with a temperature gradient. An expression is required is to describe the generated temperature distribution through the laminate. $\Delta T_{0,1}$ represents a constant and linearly-varying temperature distribution, related to the initial and final temperatures at the top and bottom of the laminate (Eq.12) and can be seen in Figure 5.

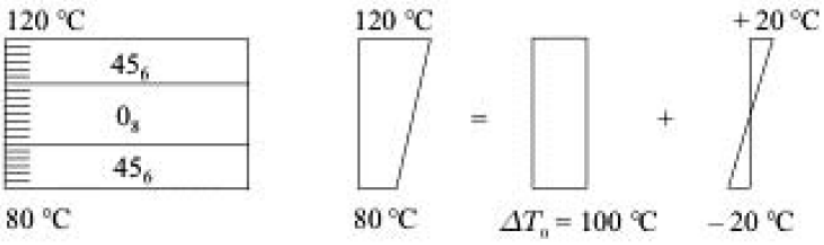

Figure 5: Representation of DT_0 and DT_1 temperature distributions [9].

$$\Delta T_0 = \frac{(T_{final\_bottom} - T_{initial\_bottom}) + (T_{final\_top} - T_{initial\_top})}{2} \tag{12}$$

$$\Delta T_1 = \frac{(T_{final\_top} - T_{initial\_top}) - (T_{final\_bottom} - T_{initial\_bottom})}{t_{ply} n_{plies}}$$

where t_{ply} is the thickness of each composite ply and n_{plies} is the number of plies at the laminate. Since the beginning of tank operation is analyzed, room temperature was considered as initial temperature. Alternatively Equation 11 can be used for temperature distribution calculation. The thermal forces associated with ΔT_o can be derived from Classical Laminate Theory (CLT), the thermal forces and moments for ΔT_1 were obtained from:

$$\begin{bmatrix} N_x^{ht} \\ N_y^{ht} \\ N_{xy}^{ht} \end{bmatrix}_{\Delta T_1} = \Delta T_1 \sum_{\kappa=1}^{n} \left(\left(\frac{z_\kappa^2 - z_{\kappa-1}^2}{2} \right) \left[\bar{Q} \right]_\kappa \begin{bmatrix} \alpha_x \\ \alpha_y \\ \alpha_{xy} \end{bmatrix}_\kappa \right),$$
$$\begin{bmatrix} M_x^{ht} \\ M_y^{ht} \\ M_{xy}^{ht} \end{bmatrix}_{\Delta T_1} = \Delta T_1 \sum_{\kappa=1}^{n} \left(\left(\frac{z_\kappa^3 - z_{\kappa-1}^3}{2} \right) \left[\bar{Q} \right]_\kappa \begin{bmatrix} \alpha_x \\ \alpha_y \\ \alpha_{xy} \end{bmatrix}_\kappa \right) \quad (13)$$

where $\left[\bar{Q} \right]_\kappa$ is the reduced stiffness matrix of each ply and α_x, α_y and α_{xy} are the thermal expansion coefficients of each at the same in-plane directions. Additionally, the hygro-thermal mid-surface strains and curvatures are given by multiplying the laminate compliance matrices with the total thermal forces and moments vector. The total strains and stresses were calculated by:

$$\begin{bmatrix} \varepsilon_x \\ \varepsilon_y \\ \varepsilon_{xy} \end{bmatrix} = \begin{bmatrix} \varepsilon_x^o \\ \varepsilon_y^o \\ \gamma_{xy}^o \end{bmatrix} + z \begin{bmatrix} \kappa_x \\ \kappa_y \\ \kappa_{xy} \end{bmatrix}, \quad \begin{bmatrix} \sigma_x \\ \sigma_y \\ \tau_{xy} \end{bmatrix} = \left[\bar{Q} \right]_k \left(\begin{bmatrix} \varepsilon_x \\ \varepsilon_y \\ \gamma_{xy} \end{bmatrix} - \Delta T \begin{bmatrix} a_x \\ a_y \\ a_{xy} \end{bmatrix} \right) \quad (14)$$

and by utilizing the transformation matrix $\mathbf{M}(a)$ (Eqn.4) stress values at each ply local materials axis system were obtained.

3.2. Intersections Reinforcement

The goal was to identify a reinforcement type that would support the structure more efficiently with the addition of minimum weight. This section deals with analyzing the concept under consideration.

An external UD carbon tow (roving) can be applied over the tank wall from the outside to the inside under tension, thus forming a ∞ sign (Figure 6). Each hoop fiber-wrapping cycle starts from the top section of the tank between the two ports at the intersection and continues to the central hollow tube covering all unreinforced junctions at longitudinal and circumferential directions. The thickness of the carbon-tow impregnated with resin is considered as 0.3mm. The inner circumference of the central hollow tube should be slightly bigger than the total arc length of all the carbon tows, which should be placed in a way that they do not overlap each other. Additionally the area where the four intersections meet and the circular tube starts should have high radius of curvature, since the entrapped hoop fibers should be stretched against the tank wall surface. This way it will keep the sub-scale tank compact and provide support without adding extra weight to the tank. Therefore the concept of having reinforcement webs at the liner and adding extra weight at the tank can be potentially dropped and thus maximizing the structural efficiency of the sub-scale tank by using hoop fibers. On the other hand there is a manufacturing challenge is posed, since the fibers must be very carefully wrapped over the intersections and the tube for an effective load transfer between the laminate membrane and the tows.

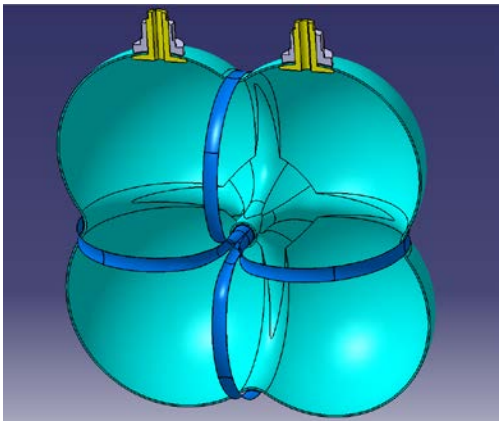

Figure 6: External UD carbon-tow at the intersection.

The highest stress concentration is expected at the vicinity of the intersections since it consists of several force components. This area is also subjected to tensile forces, since the inner pressure induces radial expansion. However since there is a complex system of forces at the intersection, free body diagrams of the laminate membrane and the hoop fibre are employed, in order to analyze the forces at meridional and hoop directions.

The intersection at the tip of the intersection can be analyzed as a ring (like a circular section of a cylindrical part) where an internal pressure is applied. The hoop membrane force per unit length of circumference can be derived as follows:

$$N_x = p \cdot r \tag{15}$$

where r equals $R_{cell} sin\varphi$ and φ is the angle between the local x-axis and the line that runs from the local origin to the intersection. However since the radius is not constant at every part of the section, the hoop force has to be re-evaluated there. Additionally there is an outward radial component at the intersection with a value of $prcos(\varphi/2)$ generated from each of the two intersecting spherical cells, where φ is depicted in Figure 7. Therefore at the mid-intersection point where the two force components meet the total force exerted by the intersecting spherical membranes in radial direction is $prcos(\varphi)$.

$$N_x' = p(r + r\cos\varphi) \tag{16}$$

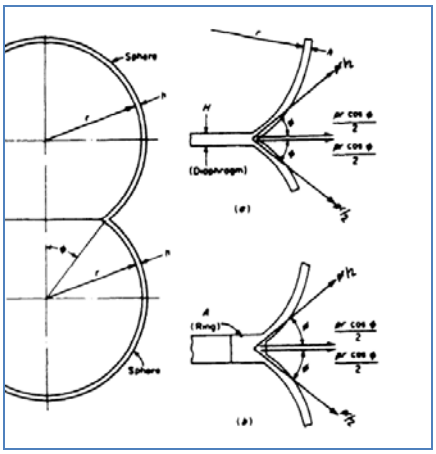

Figure 7: Forces acting at the 2 spherical cells junction [10].

At the meridional direction of the laminate membrane, the cell can be realized as a torus subjected to external pressure and also having a tension force component from neighboring spherical cells. Therefore the hoop force in the cross direction of the laminate membrane can be calculated as follows:

$$N_y = -\left(\frac{pR_m}{2}\right)\cdot\left(\frac{2a+\sin(\varphi)}{a+\sin(\varphi)}\right)+\left(\frac{pR_{cell}}{2}\right) \quad (17)$$

where a is a geometrical configuration parameter and R_m is the torus radius or basically the fillet radius at the intersection. This circumferential force has a compressive component by isolating the torus and a tensile one coming from the spherical cells. Equations 16 and 17 can be used as the load environment of the laminate at the intersection and the generated stresses at each ply can be derived from Classical Lamination Theory (CLT). The stiffness at respective directions defines the stress value, and thus the contribution of each ply to the tank. Dividing the hoop membrane force with the fibre thickness (Equation 17) generates the average axial stress of the hoop fibre.

4 FINITE ELEMENT ANALYSIS OF STRUCTURAL CONFIGURATIONS

4.1. Internal Pressure Only

This section deals with the analysis of the different steps that were carried out as well as the considerations that were taken throughout the FE analyses, taking into account only internal pressure.

A 3D axisymmetric model was built to incorporate the tank wall and basically study the structural support it provides (Figure 8). Solid tetrahedron quadratic C3D10 10-node elements were employed at the liner while tri-edron shell elements were utilized at the composite skin for the simulation at ABAQUS. The unidirectional reinforcement was considered as tied to the composite shell. The maximum expected pressure load was applied at the liner inner surface.

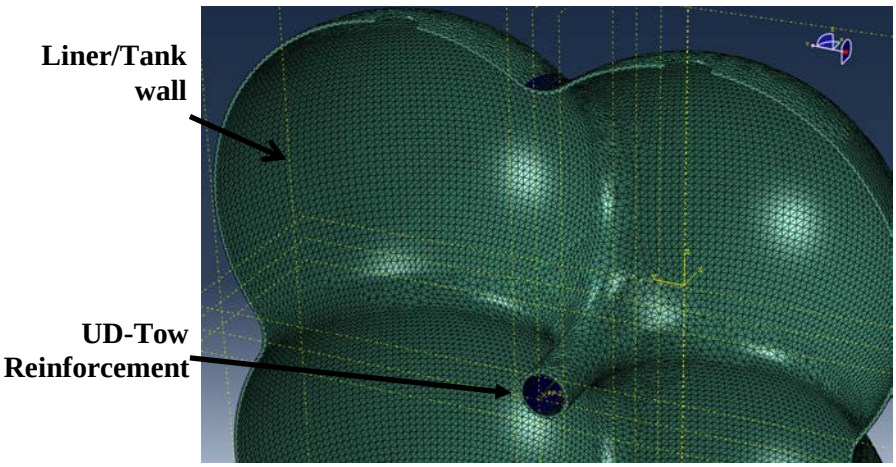

Figure 8: Model part containing liner and tank wall.

4.2. Thermal/Thermo-mechanical Loading

Section 2 states that thermal loading is induced in the tank throughout operation. Therefore it is important to isolate the effect of the thermal loading only, and study the respective tank performance. Therefor later on the counter-effect of internal pressure on the tank can be analyzed.

As a result, a coupled temperature-displacement analysis was carried at the tank, as a representative of the full tank. The tank wall and liner parts had to be partitioned several times through-the-thickness, since a one dimensional steady-state heat transfer through-the-thickness is expected throughout the analysis. Solid hexagonal linear C3D8T 8-node elements were employed at the liner and the tank wall for the simulation run at ABAQUS. A conductance interaction property as a function of distance was defined between the liner and the tank wall. The third load case (off-nominal operation after early MECO with remaining LH_2) was considered where the outside temperature was 77^{o}C, while the inside was -183^{o}C. This loading was introduced at the tank wall/reinforcement and liner respective surfaces through boundary conditions. For the case of thermo-mechanical loading the pressure load was applied at the liner inner surface. At this section a failure three-dimensional envelope was established for the proposed tank design indicating the safe operating window.

5 RESULTS

This section contains results on the subscale tank for i) internal pressure only, ii) thermal and iii) thermo-mechanical loading the composite tank wall is introduced in the analysis.

5.1. Pressure Only

Figure 9a depicts the axial and circumferential stress distribution at the spherical membrane and junction of the first ply at the composite tank wall for the highest expected internal pressure with a SF=1.5. A sufficient correlation between analytical and FE solutions can be seen. It is evident that the axial stress at the junction –where there are two different force components (explained in Section 3.2)- increases significantly. This load is distributed between the 0^o plies and the UD carbon tow (Figure 9b). The axial stress value at different locations of the UD tow from the analytical solution varies from $180 < \sigma 1 < 240$ MPa, with 240 MPa being at the intersection of the 4 rings in the center of the tank.

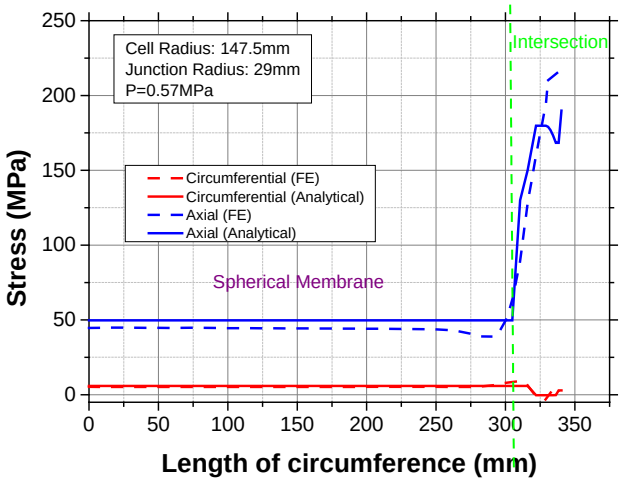

(a)

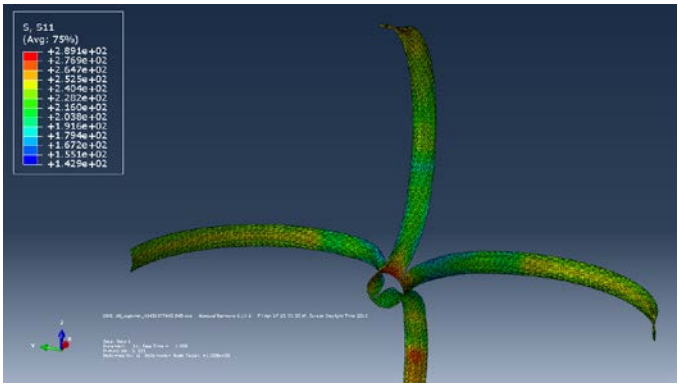

(b)

Figure 9: a) Axial and circumferential stresses at the spherical cell and intersection for ply 0 and b) axial stress for the UD fiber for *P*=0.57MPa.

5.2. Thermal Loading

Figure 10 shows a good correlation between the analytical solution and the FE solution for the temperature distribution of the composite shell through-the-thickness. It was found analytically that, when in contact; the liner and the tank wall temperature at the interface is near 0^oC for this thermal loading and this is why this temperature was used as a boundary condition. The initial temperature used was room temperature. Additionally, the respective thermal stresses at the axial direction for each ply are depicted. The FE results for thermal stresses are discrete in terms and derived from nodes, in

order to directly compare them with respective analytical results. It is clear that above room temperature the thermal stresses become compressive, which was expected since the net ΔT at that ply is positive.

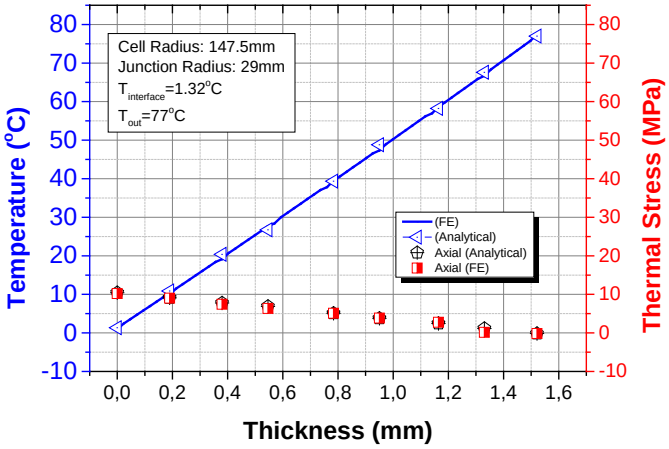

Figure 10: Temperature and axial thermal stress distribution through-the-thickness for the composite shell.

5.3. Thermo-mechanical Loading

For the case of a combined loading the inner pressure above a certain value causes a positive net radial expansion to the liner, thus forcing it to come in contact with the tank wall. This induces full load and heat transfer to the laminate. While in the spherical membranes there are equal membrane forces leading, in the junctions this is not the case, since the membrane force in the axial direction is significantly higher. The first ply (angle 0^o) according to CLT is subjected to the highest stress values associated to inner pressure since it provides the highest axial stiffness.

Figure 11 illustrates a failure envelope based on Tsai-Wu first ply failure criterion of the first ply (0^o). and the location of failure is at the longitudinal intersection. The three axes chosen were the i) uniform inner pressure, ii) the temperature at the liner/tank interface and iii) the outer temperature. It can be seen that an outer temperature range of $-100^oC < Tout < 250^oC$ and inner temperature range of $-250^oC < Tin <$ RT were chosen, while the pressure unit is in MPa (1MPa=10bar). These temperature ranges were chosen as representative for the extremes that the tank wall can be subjected to when storing a cryogenic medium (even without a liner) and at the re-entry flight stage. It is shown that the maximum allowable pressure of near 8MPa is achieved when liner/tank wall temperature is at room temperature, while the outside temperature at approximately -50^oC.

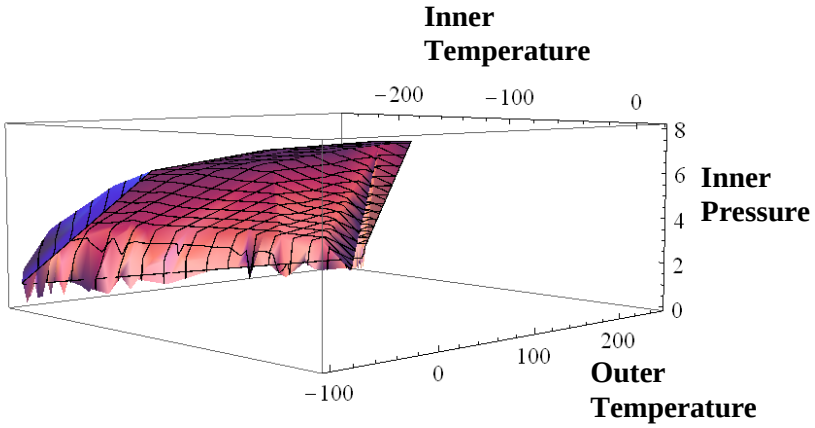

Figure 11: Three-dimensional failure envelope for 0^o ply under thermo-mechanical loading.

6 CONCLUSIONS

In the current study, the effect of the i) fiber-reinforced materials at the membrane and ii) unidimensional carbon tows at the intersections on the structural integrity of the tank was analyzed for different loading scenarios. The goal was to provide effective reinforcement at the intersections and external ports at the front ends for filling and draining of the tank, and evaluating, by using FE analysis, the structural behavior of the tank under internal pressure and thermal loading. The FE and analytical solution results showed that there is a very uniform biaxial loading of the spherical cells and localized stress concentrations at the membranes' junction. A 3D failure envelope for the first ply (angle 0^o) that is subjected to the highest stress concentration at the intersection was established. Furthermore the temperature distribution and respective thermal stresses at the composite shell were evaluated, based on the heat conduction between the liner and tank wall when they are in contact.

However a failure envelope for the whole laminate needs to be developed taking into account any secondary forces near the boundaries. Additionally the expansion of the liner with respect to the tank wall and the effect of radiation on the heat transfer between the two bodies when they separate due to difference in the coefficient of thermal expansion needs to be addressed. This is generally the case, when a cryogenic medium is stored and the inner pressure has a small value. Finally the effect of quasi-static inertia loads (gravitational accelerations) needs to be analyzed, and the effect on the tank supports.

ACKNOWLEDGMENTS

This work has been performed within the 'Cryogenic Hypersonic Advanced Tank Technologies' project investigating tank technologies for high-speed transport. CHATT, coordinated by DLR-SART, is supported by the EU within the 7th Framework Program Theme 7 Transport, Contract no.: ACP1-GA-2011-285117. Further information on CHATT can be found on http://www.chatt.aero. Furthermore we would like to thank Tim Vlaar for technical support.

REFERENCES

[1] M. Sippel and A.van Foreest, SpaceLiner Rocket-Powered High-Speed Passenger Transportation Concept Evolving in FAST20XX, *Proceedings of the 61st International Astronautical Congress*, Prague, 2010.

[2] F.J.J.M.M. Geuskens, O.K. Bergsma, S. Koussios and A. Beukers, Analysis of Conformable Pressure Vessels: Introducing the Multibubble, *AIAA Journal*, **49**, 2011, pp. 1683-1691.

[3] V.V. Vasiliev, *Composite Pressure Vessels: Analysis, Design and Manufacturing*, Bull Ridge Publishing, 2009.

[4] W.C. Bert, Large Weight Reductions Possible in Pressure Vessels, *Space/Aeronautics*, **38**, 1962, pp. 77–83.

[5] V.A. Komarov, Multicell Reservoir, *Mechanics of Solids*, **5**, 1970, pp. 181–183.

[6] M. Sippel, A. Kopp, K. Sinko and D. Mattsson, Advanced Hypersonic Cryo-Tanks Research in CHATT, *Proceedings of the 18th AIAA International Space Planes and Hypersonic Systems and Technologies Conference*, France, 2012.

[7] A. Haaland, High-Pressure Conformable Hydrogen Storage for Fuel Cell Vehicles, *Proceedings of the U.S. DOE Hydrogen Program Review, California*, 2000, pp. 463-469.

[8] S.T. Peters, *Composite Filament Winding*, ASM International Materials Park, 2011.

[9] L.P. Kollar and G.S. Springer, *Mechanics of Composite Structures*, Cambridge University Press, 2003.

[10] D.M. Fryer and J.F. Harvey, *High Pressure Vessels*, Chapman & Hall, 1998.